Monitoring tumor response to radiation therapy with longitudinal and multimodal molecular imaging

Master's project in Life Sciences and Technology

Carried out in the
Imaging Radiobiology Laboratory
At
Stanford University
Under the supervision of
Prof. Edward Graves, PhD

Under the direction of
Prof. Freddy Radtke, PhD
At the
Swiss Institute for Experimental Cancer Research (ISREC)
EPFL

Jessica Perez

School of Life Sciences

Swiss Federal Institute of Technology Lausanne

September 2010

Acknowledgements

I would like to thank Prof. Edward Graves for giving me the great opportunity to come to Stanford, and for his support throughout my stay, Marta Vilalta who spent so much time explaining and teaching me all the different techniques I learned, Geoffrey Nelson, Rehan Ali, Magdalena Bazalova, Matt Noll for their help with imaging and all the members of the Graves lab, who welcomed me, and who made this year, an amazing year.

I would like to thank my supervisor, Prof. Freddy Radtke, for his mentoring and support during this year, the life sciences faculty for allowing these mobility programs, and EPFL.

I would also like to thank my parents who made my coming here possible and all my family and friends for their precious support.

Abstract

Purpose

Metabolic changes induced by radiation therapy (RT) provide a biological measure of tumor response to treatment beyond anatomic changes. In this preclinical study we investigated these changes through longitudinal monitoring of tumor response to varying doses of RT with ^{18}F-Fluorodeoxyglucose Positron Emission Tomography (FDG-PET) and Computed Tomography (CT), as well as bioluminescence imaging (BLI). We sought to establish the metabolic alterations in irradiated tumors at early timepoints following treatment.

Materials & Methods

Human HT-29 colon carcinoma cells were inoculated subcutaneously on both sides of the back of nude mice. Tumors were grown for two or three weeks. One tumor per animal was treated with 10 or 20 Gy of RT on day 0. The first ten mice were imaged with both FDG-PET and CT on day -1, 1, 3, 9, and 14. The other 10 mice were imaged with BLI once a week during tumor growth and on the same days as the PET-CT study. These findings were correlated with histology.

Results

At the beginning of treatment tumors exhibited low FDG uptake. The volume of the treated tumors (TT) determined by CT images, remained stable or decreased (for dose of 20 Gy), whereas the untreated tumors (UT) continued growing. Surprisingly, 9 days after RT, the FDG-uptake increased in the TT and remained low in the UT. We observed a clear decrease in BLI signal in TTs appearing also 9 days after RT.

Conclusion

We have applied preclinical imaging and radiotherapy methods to study tumor response to treatment. The surprising rise in FDG uptake at day 9 after RT could be the result of several mechanisms including inflammation, that still remains to be determined with immunohistochemistry. This study raises the possibility of FDG PET producing false negatives for early response. The preliminary data reported here will be used to establish future technical and biological approaches towards monitoring cancer therapies.

Contents

List of Figures

Chapter 1

Introduction

1.1 Purpose

The purpose of this study is to describe the effects of radiation therapy (RT) on tumor growth and metabolism using different imaging modalities. Performing a longitudinal study with repeated measurements of a subject over a certain period of time, allows us to assess the kinetics of tumor response to RT. This can give a better idea of the time scale of occurring events, as molecular and anatomical changes as seen by the different imaging tools do not always occur at the same time. In addition, this study investigates the impact of tumor size and radiation dose on imaging tumor response. Those factors can influence the outcome of the tumor, and therefore its reaction to imaging.

1.2 Assessment of tumor response to RT with molecular imaging

In clinical radiation oncology, the most common way to assess tumor response to treatment continues to be by examination of changes in the size of the tumor with anatomical imaging modalities such as computed tomography (CT) or magnetic resonance imaging (MRI). These anatomical changes in response to therapy, typically shrinkage of the tumor mass, appear late in the course of treatment, and do

not reflect the underlying molecular changes occurring much earlier [1, 2]. Understanding the early reactions of tumors to radiation therapy (RT) allows for the fine tuning of the treatment plan in a patient specific manner. If the treatment does not yield the expected results, an awareness of the negative response early within the treatment period allows adjustments to be made to the therapy protocol early on. Tumors exhibit a high degree of biological heterogeneity, and as a result, patients diagnosed with the same tumor type often do not react similarly to the same therapy. Detecting molecular level changes in response to RT could potentially assist with choosing or changing a treatment protocol.

Positron emission tomography (PET) has emerged as a powerful molecular imaging tool for diagnosis, treatment planning, and monitoring response of multiple cancer types. It allows the use of a variety of radiotracers to assess different tumor parameters, the most common being ^{18}F-fluorodeoxyglucose (FDG) which monitors changes in glucose metabolism. FDG highlights cancer cells, which are more metabolically active than many non-cancerous cell types, and therefore exhibits higher glucose consumption than the rest of the body. FDG-PET is already used for monitoring therapy response in multiple cancer types [3, 4, 5]. However the molecular effects of RT, and their impact on imaging, remain poorly understood. The availability of pre-clinical models for the study of RT is a valuable tool in understanding the molecular events occurring in response to therapy. Furthermore, non-invasive molecular imaging allows the longitudinal *in vivo* study of the same subject over time which provides a great advantage for determining treatment follow up. PET imaging for the assessment of tumor response to RT has been evaluated with FDG as well as with other tracers such as 18-F-fluorodeoxythymidine (FLT), a proliferation marker [6]. Results showed consistent decrease in FLT uptake after RT, but contradictory results for FDG whose uptake can be either increased [7] or decreased [8] in response to treatment.

Cancer cells within a tumor are not all identical. They also interact with their environment and modify it. This results in a heterogeneous tumor mass with different regions harboring different parameters such as variable hypoxia or aberrant vasculature. These different regions can react in various ways when treated with radiation [9]. Regions of low oxygen within tumors appear more resistant to radiation and are therefore important to image. Imaging hypoxia can

be done using PET with different hypoxia tracers such as Cu-ATSM, FMISO, FAZA or EF5 [10]. Tumor heterogeneities as a result of RT include regions of pronounced cell death, necrosis or fibrosis formation which can be investigated with different molecular imaging techniques such as proton magnetic resonance spectroscopy (MRS) or diffusion weighted (DW) MRI [11], and ultrasound (US) [12].

An advantage of pre-clinical animal models is the use of reporter genes for optical imaging using techniques such as bioluminescence imaging (BLI). Cancer cells expressing luciferase can be monitored non-invasively and allow the assessment of tumor growth or shrinkage *in vivo* [13, 14].

Altogether, the assessment of tumor response to radiation therapy is complex as it relies on many parameters such as cancer type, subject, tumor heterogeneity or tumor microenvironment. Using available tools in molecular imaging, it is possible to study the effects of radiation on some precise aspects of a tumor.

1.3 Molecular Imaging

> "Molecular imaging is the visualization, characterization, and measurement of biological processes at the molecular and cellular levels in humans and other living systems. To elaborate; molecular imaging typically includes 2- or 3-dimensional imaging as well as quantification over time. The techniques used include radiotracer imaging/nuclear medicine, MR imaging, MR spectroscopy, optical imaging, ultrasound, and others." D.A. Mankoff [15]

1.3.1 Positron Emission Tomography (PET)

The principle of PET is the administration of positron emitting radionuclide to a subject. The radioisotope emits a positron, as part of its decay process, which travels a short distance before annihilation caused by electron interaction. This process results in the emission of two $511\,keV$ photons going in opposite directions. The detectors, which are arranged in a circle around the subject, registers a signal only if two $511\,keV$ photons are detected within an interval of

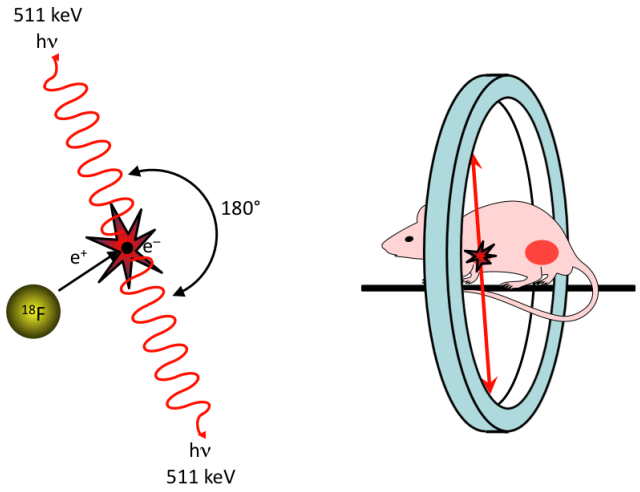

Figure 1.1: Principle of PET.

approximately 20 ns on opposite collinear detectors. It is then possible to retrace back where the annihilation event had occurred and reconstruct an image (Figure 1.1[1]) [16].

^{18}F-Fluorodeoxyglucose (FDG) PET

FDG is a glucose analog labeled with the radioactive isotope fluorine-18. It acts as glucose in the body except that after cellular uptake, it gets stuck in the second step of glycolysis and accumulates in the cell (Figure 1.2[1]). FDG PET therefore allows monitoring of glucose uptake and metabolism by cells in the body. The more cells are metabolically active, the more FDG uptake that is observed and the stronger the signal in PET. This technique can, highlight the regions of high glucose uptake and consequently tumors which have a high cellular activity [17]. Although it is not strictly tumor specific, FDG PET is a good marker of high cellular metabolism, which is of importance for several types of cancer, and is the only PET tracer approved by the FDA for use on a regular basis in the clinic.

[1]Courtesy of Prof. E. Graves

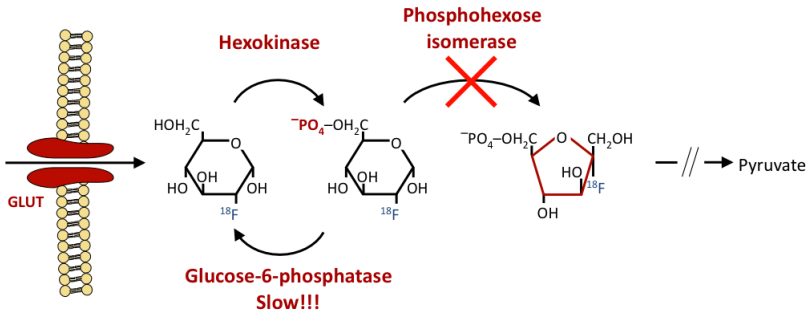

Figure 1.2: FDG cell trapping mechanism.

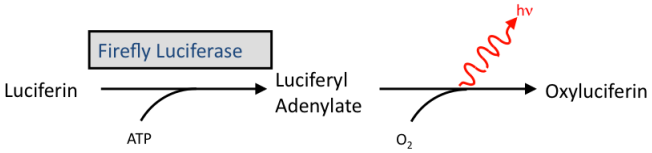

Figure 1.3: Principle of BLI.

1.3.2 Bioluminescence imaging (BLI)

Bioluminescence imaging is a powerful tool that allows the *in vivo* monitoring of cells expressing luciferase. Luciferase is an enzyme that reacts with its substrate, luciferin, and in the presence of oxygen, emits photons (Figure 1.3[1]) that can be measured using a sensitive charge coupled device (CCD) camera. Luciferin is not available in mammals, so it has to be injected prior to imaging. BLI is a useful method, as it can be used to non-invasively monitor luciferase expression both by constitutively expression to assess live cells, and as a reporter gene for a chosen specific promoter. For cancer research, cells labeled with luciferase can be injected in mice to form tumors, whose evolution and growth can be subsequently followed *in vivo* with BLI [13].

1.4 Radiation Therapy (RT)

About half of all cancer patients are treated with radiotherapy at some point during the course of treatment [18]. RT is the treatment of cancer with the use of ionizing radiation. A beam of electromagnetic radiation (or photons) is

directed to the tumor site with energies ranging from $100\,keV$ to several MeV. Photons of this level of energy are able to eject electrons from atoms constituting molecules in a process called ionization. Ejected electrons cause further ionization when colliding with other molecules. Most of the damage from RT is done by intracellular ionized molecules which become reactive, as they cause a succession of chemical reactions that lead to chemical bond breaks. Those breaks occur in all cellular molecules, including DNA, which is very sensitive to damage due to it having only two copies and a slow turnover compared to other macromolecules. DNA damages activate the very efficient DNA repair pathways of cells, but if the damage is too great, cells die. As tumor cells are prone to having impaired DNA repair or cell cycle arrest functions, if the DNA is not sufficiently repaired before division, it can lead to chromosomal aberrations and mitotic catastrophe. The idea is to induce damages that are fatal to tumor cells while reparable for normal tissue that will not divide unless DNA is repaired. The dose of radiation is measured in Gray (Gy) units [19, 20].

> "To give an idea of the scale of damage, $1\,Gy$ of irradiation will cause in each cell approximately 10^5 ionizations, more than 1000 damages to DNA bases, around 1000 single-strand DNA breaks (SSBs) and around 20-40 double-strand DNA breaks (DSBs). To put this into further perspective, $1\,Gy$ will kill only about 30 percent of cells for a typical mammalian cell line, including human." M.C. Joiner and AJ Van der Kogel [20]

Usually RT is delivered to a target volume previously determined with treatment planning based on imaging. The dose is delivered from multiple angles to optimize the dose to the target while sparing normal tissue as much as possible. The total dose of RT is commonly split into multiple fractions of low dose, primarily to allow normal tissue to recover. Typically, an average clinical RT would involve $2\,Gy$ per day, five days a week, for about 5 weeks [20].

1.5 Research focus

Multimodality imaging allow the visualization of different aspects of tumor response to treatment. FDG-PET-CT and BLI were used in a study for monitoring chemotherapy (IL-18-Binding protein-Fc therapy) response in lung metastasis mouse model. All imaging techniques showed an inhibition of tumor progression when treated with the tested drug [21]. In another study, FDG-PET was used to analyze the effects of a pre-treatment scan on increasing radiation dose in a head & neck cancer xenograft mouse model. Results demonstrated that tumors with higher FDG uptake prior to treatment were more responsive to increasing RT dose than those with a lower initial FDG uptake [22]. In addition, different PET tracers were evaluated for monitoring tumor response to RT in pre-clinical mouse models. This study showed the potential of FMT (O-$^{1}8F$-Fluoromethyl-D-tyrosine) as an early marker for RT response when compared with FDG or FLT [7]. Altogether, the studies discussed above create the ground for assessing tumor response to RT with multimodal imaging.

In this study, a colorectal carcinoma xenograft mouse model was used to assess tumor response to different doses of RT with FDG-PET-CT and BLI. In this case, growth and metabolic activity of cancer cells were investigated before and serially after treatment. Imaging findings were also correlated with histology.

Chapter 2

Materials & Methods

2.1 Cell culture

HT-29 cells (colorectal carcinoma) were thawed and seeded on a large cell culture dish with 20 ml of Mc Coy's medium with 10% fetal bovine serum (FBS) and grown in 5% CO_2 at 37°C in a humidified incubator. Growth media was changed 3 times per week and cells were trypsinized when they were confluent (See Appendix A.1 for more details).

Other cells lines were also cultured for previous experiments, and include FaDu cells (Head & Neck squamous cell carcinoma) and MDA-MB-468 cells (breast cancer) both expressing luciferase constitutively. Those cells were grown with Dulbecco's Minimum Essential Medium (DMEM) with 10% FBS.

2.1.1 Cell transduction

Photinus pyralis (*firefly*) luciferase under the control of the citomegalovirus (CMV) promoter retrovirus was kindly provided by the group of Professor AJ Giaccia (Stanford University, CA, USA). Cells were grown in culture dish, growth medium was removed, 1.5 ml of retrovirus with 2 μl polybrene was added to the culture, and left overnight. The retrovirus were removed the next day and cells were seeded on a new cell culture dish with growth medium.

2.2 Tumor model

The tumor model used for these studies was human colon carcinoma mouse xenograft. HT-29 cells were cultured, and counted using a Neubauer chamber (See Appendix A.2). One million cells were used for each injection. Nude mice were anesthetized with 2% isoflurane and 4 L/min of oxygen, and cells were injected subcutaneously in the back. Tumors were allowed to grow for 2 to 3 weeks.

Previous experiments using the FaDu and MDA-MB-468 cell lines showed no tumor formation *in vivo* (in 4 and 5 mice, respectively), and were therefore not used further in this study. This can be due to several factors such as a contamination of cells with mycoplasma, and the presence of the luciferase gene (which seems unlikely as cells were growing normally in culture), or failed injection of cells into mice.

2.3 PET-CT Imaging

2.3.1 Outline of experiments

To investigate the differences between anatomical and metabolical changes in tumors when treated with RT, mice were inoculated with HT-29 human colon carcinoma cells to form two subcutaneous tumor xenografts per animal. One tumor per mouse was treated (Treated Tumor: TT), and the other served as an internal control (Untreated Tumor: UT). Tumor responses were studied for multiple RT doses and across time. Imaging was performed on day -1 (baseline), treatment on day 0, and imaging again on day 1, 3, 9 and 14 after RT.

A first study was performed on 15 mice divided into 3 groups of 4 animals treated with 5, 10 or 20 Gy, and 3 unirradiated control mice. The imaging was performed using a bed holder allowing the simultaneous imaging of 4 mice both with PET and CT. Due to the occurrence of multiple problems during this experiment, some modifications were made to improve the protocol, and the study was repeated. These are discussed in section 3.1

A second study investigated the impact of initial tumor size in imaging RT response. This involved 10 nude mice, 5 of which were inoculated with cells

2 weeks before RT and the other 5 mice inoculated 3 weeks before RT, which resulted in small (ranging from 2 to $4\,mm^2$) and big tumors (ranging from 6 to $8\,mm^2$) respectively. The mice were divided into four groups of two animals each: small tumors treated with $10\,Gy$, small tumors treated with $20\,Gy$, big tumors treated with $10\,Gy$ and big tumors treated with $20\,Gy$. One untreated big tumor and one untreated small tumor were used as controls. In this case, mice were imaged using two different mouse beds for image registration. These comprised one simple plastic bed and a more complex bed with fiducial markers which were visible on both CT and PET images. The latter was developed by a colleague, Geoffrey Nelson (Graves laboratory) and tested here for validation.

2.3.2 FDG-PET

Mice were anesthetized with 2% isoflurane and $4\,L/min$ of oxygen in a knock down box and kept under anesthesia using a nose cone during the radiotracer injection and imaging. The FDG vial was placed in a lead pig and all manipulations involving the radiotracer were performed behind a lead shield. $200\,\mu Ci$ of FDG was injected intraperitoneally 1 hour before imaging. The remaining radioactivity in the syringe used for injection was measured to deduce the exact amount of injected activity. Mice were kept under anesthesia and warmed for 1 hour before imaging. They were then placed on a movable mouse bed, and 10 minute static PET images were acquired on a R4 microPET (Concorde Microsystems, knoxville, TN, USA). These were automatically reconstructed with OSEM 2D.

2.3.3 CT imaging

Once the PET images were acquired, the anesthetized mice were directly transferred using the mouse bed to the CT scanner (Gamma-Medica Ideas, Northridge, CA, USA), and a 1 minute scan was performed with the X-ray tube operating at a current of $225\,\mu A$ and a voltage of $75\,kVp$. Acquired images were subsequently reconstructed using filtered back projection with a voxel size of $0.17\,mm$ and a field of view of $110\,mm$.

2.3.4 Image analysis and quantification

PET and CT images were analyzed using RT_Image software [1] [23] using the procedures described below.

PET-CT image registration

In preliminary studies, imaging was performed with a 4 mice bed. This allowed higher throughput mouse imaging, but it was difficult to co-register the acquired PET and CT images. Registering those images has to take into account 6 degrees of freedom for translation and 6 for rotation, as well as breathing motion and mouse-specific displacement when moved from the PET to the CT scanner. The latter effects are difficult to account for, as registration is typically performed by applying transformations across the entire image. Inaccurate image registration can lead to imprecise quantification. In the presented results, all mice were imaged individually, to minimize registration errors.

In the final study, mice were imaged individually. For each mouse and each timepoint, PET images were overlaid on the CT images, using visual inspection for the simple bed or a point matching algorithm with fiducial markers. PET images were normalized with a calibration factor of $1250\,\mu Ci/ml$, and converted to percent injected dose per gram ($\%ID/g$) using the following equation [24].

$$\%ID/g = (\frac{Activity\ in\ a\ gram\ of\ tissue}{Injected\ dose}) * 100 \tag{2.1}$$

The fused images were then saved in DICOM format for subsequent analysis. Figure 2.1 shows sample PET-CT images.

Tumor region of interest quantification

Based on the overlaid PET-CT images, tumor region of interests (ROIs) were manually drawn on coronal view images for multiple slices and subsequently interpolated to encompass the whole tumor volume. Based on these ROIs, datas such as tumor volume, mean or $90th$ percentile FDG uptake were computed.

[1] http://rtimage.sourceforge.net/

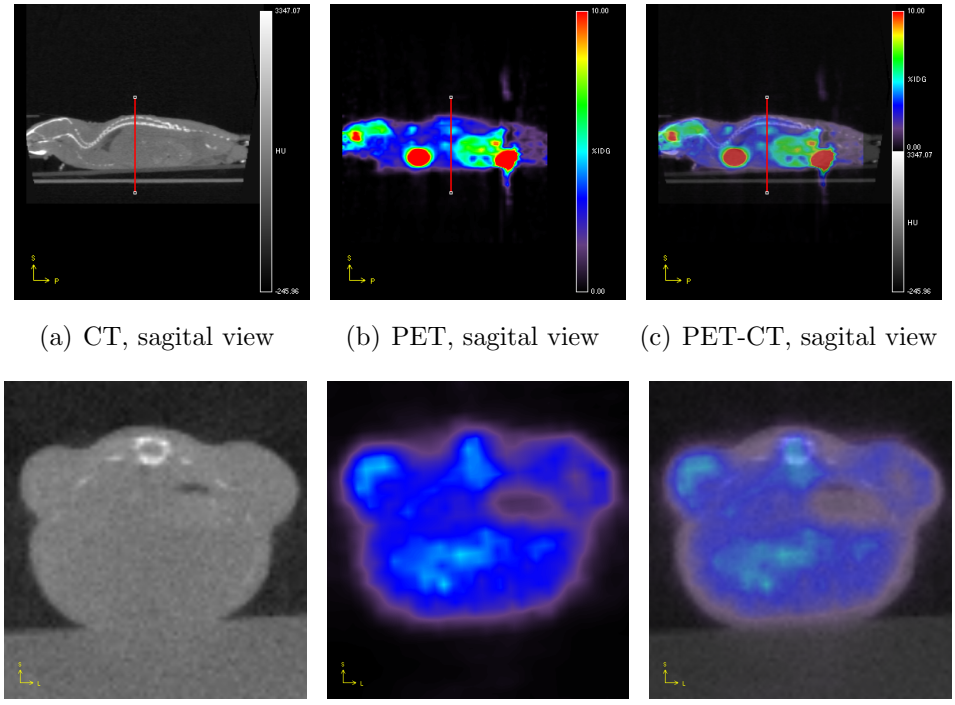

(a) CT, sagital view (b) PET, sagital view (c) PET-CT, sagital view

(d) CT, coronal view (e) PET, coronal view (f) PET-CT, coronal view

Figure 2.1: PET-CT fusion in sagital and coronal views. *Red line indicates the coronal view.*

2.4 Bioluminescence Imaging (BLI)

2.4.1 Outline of experiments

To investigate the kinetics of tumor growth and cell killing after RT, nude mice were inoculated with HT-29 cells constitutively expressing luciferase. Each mouse bared two subcutaneous tumors, one treated and one untreated (TT and UT, respectively).

A pilot study with 5 mice was performed, but the irradiator was out of order for 5 days at the time the tumors had to be treated. This delay caused the tumors to become too big for a two weeks follow up period after RT, and therefore had to be sacrificed before any relevant results were obtained.

This final study involved ten nude mice separated into two groups of four. Two mice were kept as completely untreated controls. One group received a dose of $10\,Gy$ in one tumor, and the other group received $20\,Gy$. Both tumor growth and response to RT were monitored as mice were imaged on day 2, 8, 13, 15, 17, 23, and 30 after cell inoculation. Treatment was delivered on day 14.

2.4.2 BLI

Mice were anesthetized with 2% isoflurane and $3\,L/min$ of oxygen, then injected intraperitonealy with $2.5\,\mu g$ of luciferin (at concentration $16.7\,mg/ml$), and placed immediately in the imaging chamber of an IVIS200 (Caliper life sciences, Alameda, CA, USA), where 5 mice were simultaneously kept under anesthesia using nose cones. A bioluminescence image was acquired 15 minutes after luciferin injection, using 30 seconds exposure time, medium binning, and the largest field of view. The bioluminescence image was then automatically superimposed on a grayscale photograph, and visualized using a color map.

2.4.3 Image analysis and quantification

Images were analyzed with Living Image 4.0 software. An elliptical ROI was drawn on each tumor and the average radiance (in $p/sec/cm^2/sr$) as well as the total flux (in p/sec) was computed.

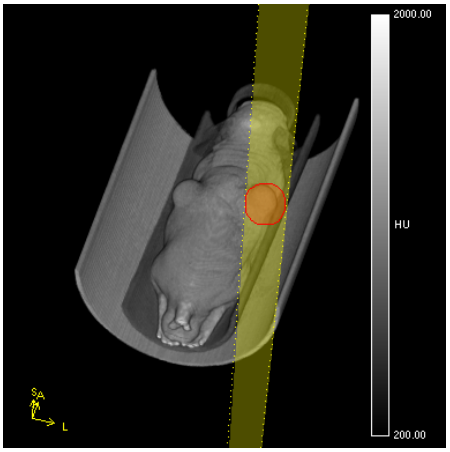

Figure 2.2: Representation of RT delivery

2.5 Radiation Therapy (RT)

Mice were anesthetized with an intraperitoneal injection of ketamine-xylazine solution (8.6% ketamine, 8.6% xylazine in PBS; 10 μl per gram of mouse). Radiation delivery was performed using a single field irradiator that consisted of a treatment table and an RT 250 x-ray tube that was operated 200 kVp with a current of 17 mA. The dose rate of the system is approximately 30 Gy/h. The mice were positioned under a lead shield (thickness: 1/8 $inch$ or 3.175 mm) containing 1 cm apertures where the tumors to be irradiated were placed. For each mouse, one tumor was irradiated with 10 Gy or 20 Gy and the other remained untreated (Figure 2.2).

2.6 Histology

To further investigate the results obtained with *in vivo* imaging, immunohistochemistry was performed for different relevant markers such as Ki67 for proliferation, CD-68 for inflammation and CD-34 for vasculature. Only the big tumors imaged with PET-CT (2 TTs and 2 UTs) were analyzed.

2.6.1 Tissue sample preparation

When the study was completed, mice were sacrificed with CO_2. Tumors were collected, and fixed in 10% formaldehyde at 4°C for 24 hours. Tumors were embedded in paraffin, and sliced at $4\,\mu m$. Two sections per tumor were stained with hematoxylin and eosin to assess tissue architecture, and unstained slides were used for subsequent immunohistochemistry.

2.6.2 Immunohistochemistry (IHC)

Ki67

Tissue samples were stained with Ki67 using the Avidin Biotin peroxidase method, for both treated and untreated tumors. The first antibody was anti-Ki67, anti-human made in rabbit (1:250), and was left overnight at $4\,°C$. The secondary biotinylated antibody was added the next day for 1 hour, goat anti-rabbit (1:200). The third Avidin/Streptavidin antibody conjugated to HRP was applied for 30 minutes (1:200). Signal was developped with DAB peroxidase. Sections were also stained with hematoxylin. (See Appendix B for protocols)

CD-68 and CD-34

The immunohistochemistry protocol was similar to the Ki67 described above. The primary antibodies were anti-CD-68 and anti-CD-34 anti-mouse made in rat. Multiple variations of the staining protocol were tried, including different concentration of the primary antibody (1:100, 1:250), two different secondary antibodies (one made in goat and the other in donkey), and multiple repeats of the experiment.

2.6.3 Staining quantification

Tissue staining was visualized using a microscope (Leica Microsystems GmbH, Wetzler, Germany), and typically 3 pictures were taken at different areas within the sample. The percent of brown staining on each image was calculated, and averaged to obtain a percent area of staining for each sample section.

Chapter 3

Results

3.1 FDG-PET-CT Imaging

3.1.1 Preliminary studies

An initial study was performed, during which multiple problems were encountered. The CT scanner was out of order for the baseline scan before RT, and therefore, no anatomical information was acquired that day. The tumors were barely visible on the PET images, and the use of a 4 mice bed holder made ROI determination difficult. This made it difficult to detect potential changes in FDG uptake. One week after RT, 5 mice (4 treated with $20\,Gy$ and 1 untreated, in the same cage) died. The results from this study were not conclusive, but it provided the opportunity to make some changes and improve the outcome of the follow-up experiment. It was decided that RT would be delayed so that the resulting bigger tumors would be more visible on the PET images. In addition, mice were imaged individually to allow better image registration.

The results presented here, are from the final study described in Section 2.3.1.

3.1.2 CT Tumor volume

Based on the CT images, it was possible to monitor tumor volume changes during all the monitored timepoints. We observed that the UT continued their exponential growth during the time of the experiment as shown by model fitting (Figure

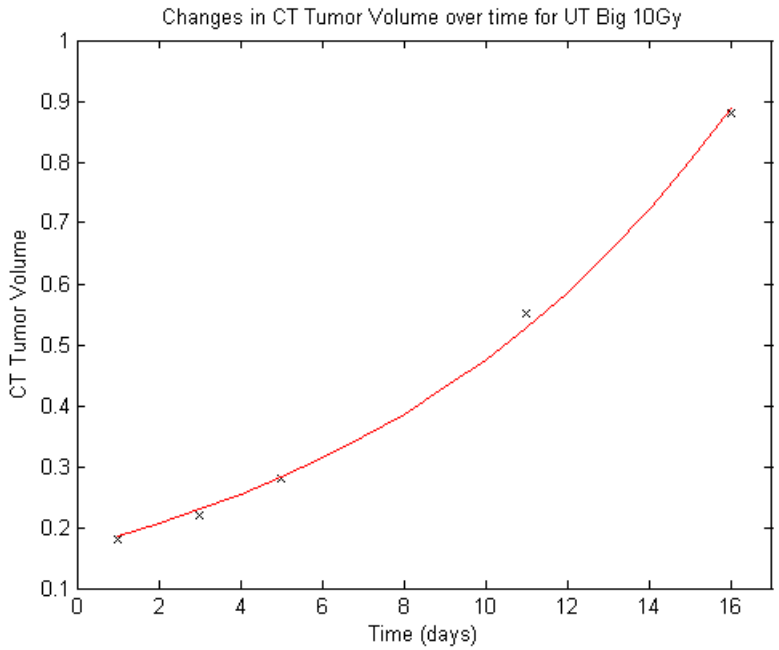

Figure 3.1: Exponential curve fitting CT tumor volume measurements

3.1). The TT showed a stabilization of tumor size for the group treated with a dose of $10\,Gy$, and a decrease in tumor size for the groups treated with $20\,Gy$ (Figure 3.2). We could not conclude anything for the small tumors group treated with $10\,Gy$ because the tumor volumes were very small and therefore ROI determination was too subjective. This difference in tumor volume between treated and untreated was visible at day 9 only for the small tumors group treated with $20\,Gy$, and appeared later (at day 14) for the other groups (Figure 3.2).

3.1.3 FDG-PET

At the baseline, FDG uptake was low in the HT-29 tumor model (Figure 3.3(a)). Interestingly, at day 9 after RT, we could observe an increase in FDG consumption in TTs only (Figure 3.3(d)). In one case, the increased signal remained after 14 days, whereas in others, the signal decreased again at day 14. This result was confirmed by computing the $90th$ percentile of tumor FDG uptake. The TT over UT ratio (TT/UT) reached an average of 1.3 on day 9 after RT (Figure 3.4(a)).

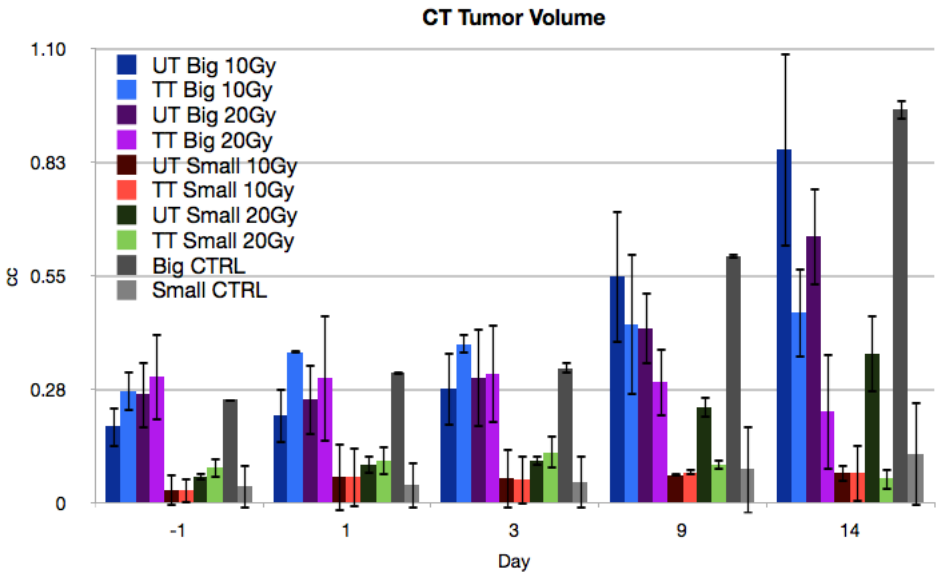

Figure 3.2: CT tumor volumes. UT volume (darker colors) increases whereas TT volume (brighter colors) remains stable or decreases.

The increase in FDG uptake was observed for all subjects, but was stronger in big tumors regardless of the dose received.

3.2 Histology

To further assess why tumor FDG uptake was increased after RT, UTs and TTs were harvested after the study was completed, embedded in paraffin, sliced and stained using three different markers. We used an anti-Ki67 antibody, which stained for proliferating cells and allowed us to see if the increased FDG uptake could be due to accelerated repopulation after RT. We also labeled CD-34, a marker of endothelial cells, to assess the vasculature and angiogenesis process, and CD-68, a macrophage marker, to monitor inflammation.

3.2.1 Tumor size

Tissue sections reflected findings from the CT images in terms of tumor size. We observed that TTs that received a dose of $20\,Gy$ were much smaller than UTs

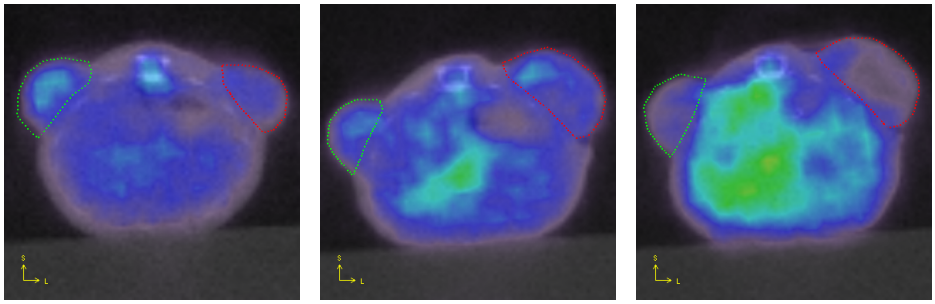

(a) Day -1 (b) Day 1 (c) Day 3

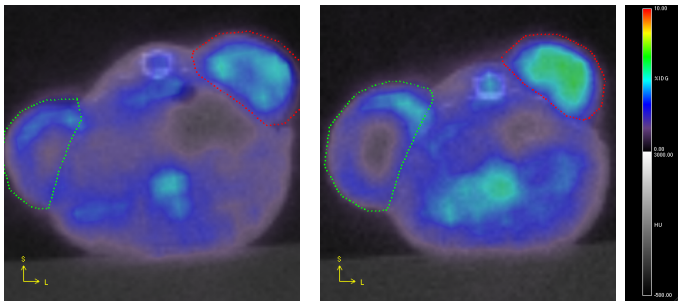

(d) Day 9 (e) Day 14

Figure 3.3: Series of PET-CT images of a representative mouse, coronal view. Tumor FDG uptake is low, but there is an increase in FDG uptake in the TT on day 9 after RT. A central region not uptaking FDG appears when the UT tumor reached a certain size on day 9.*Green ROI: UT, Red ROI: TT.*

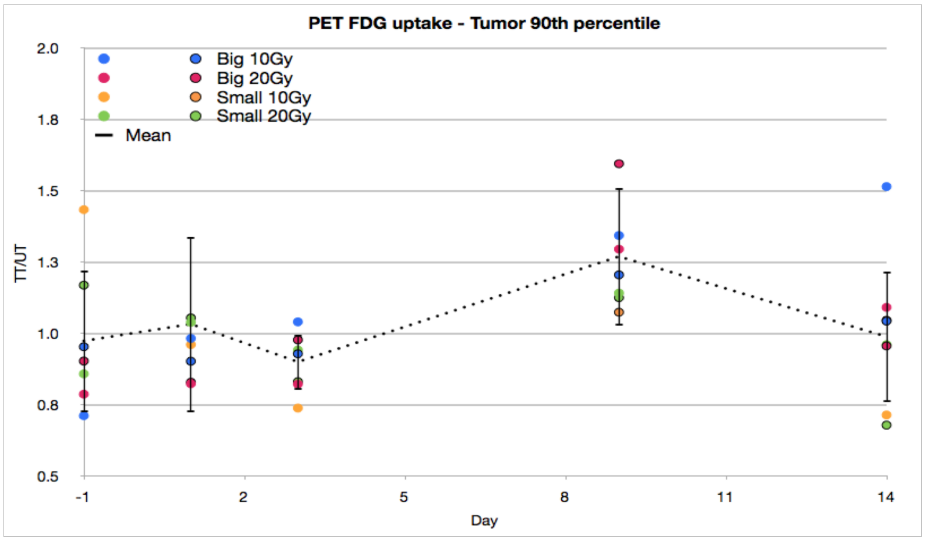

(a) Mean TT/UT

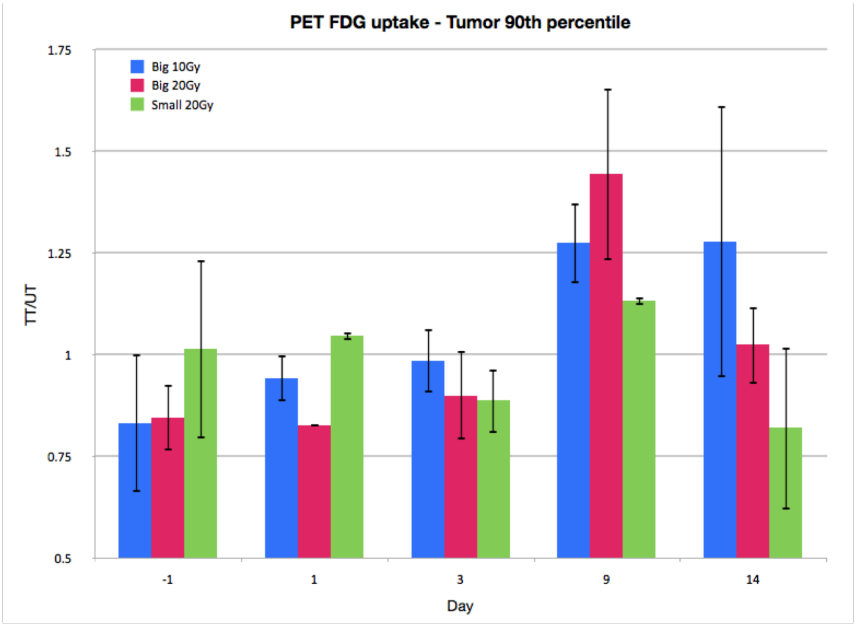

(b) TT/UT for each group

Figure 3.4: TT/UT ratio of tumor $90th$ percentile of FDG uptake across all imaging timepoints. There is an increased FDG uptake in the TT at day 9 after RT.

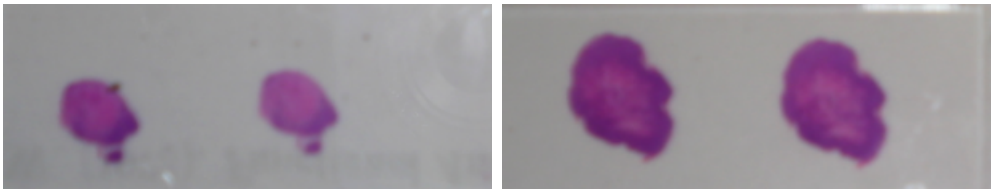

(a) TT and UT: 20 Gy

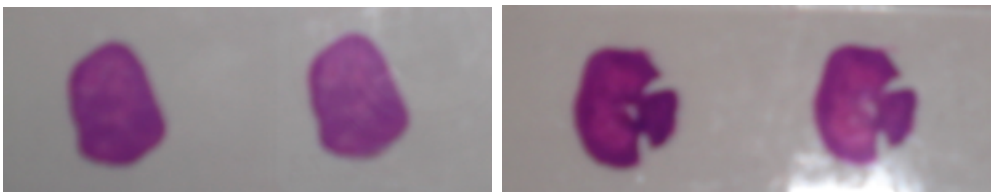

(b) TT and UT: 10 Gy

Figure 3.5: Picture of representative tumor sections

(Figure 3.5(a)). This difference was not observed in the TTs that received 10 Gy (Figure 3.5(b)).

3.2.2 Hematoxylin and Eosin (tissue architecture)

The hematoxylin and eosin (HE) staining showed heterogeneities within the tumor mass (Figure 3.6). Specifically, we observed a central necrotic region (in (a)) surrounded by a rim of living cells (in (b)). These findings were supported by the PET data (Figure 3.3(d)).

3.2.3 Ki67 (proliferation)

Ki67 staining showed that tumor mass was very heterogeneous with an unproliferating central region corresponding to necrotic regions and a rim of proliferating cells on the edge of the tumor which correspond nicely with the HE staining. The larger UTs showed more necrosis and therefore less proliferative centers. Figure 3.7 shows Ki67 staining for UT (a) and TT (b) with unproliferating regions in the center (left), and proliferating regions on the edges (right).

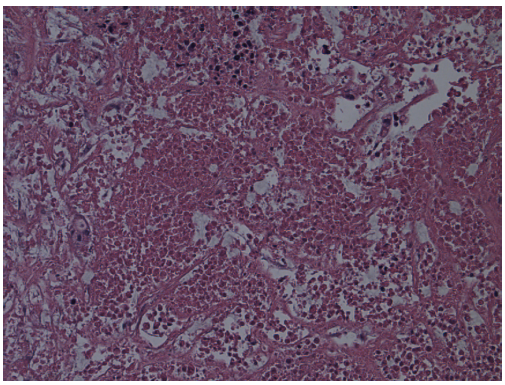

(a) Necrotic center

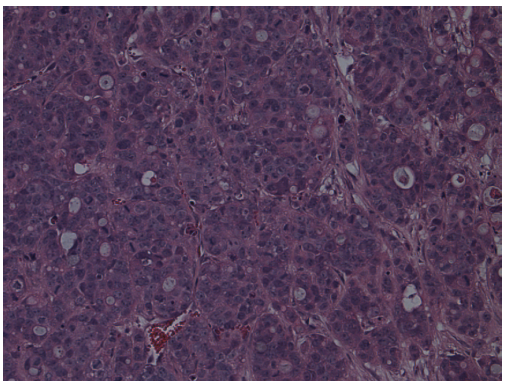

(b) Rim of cells

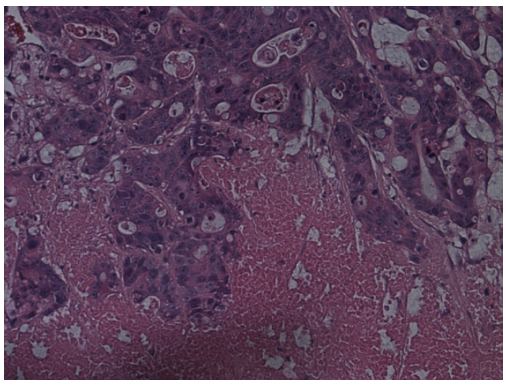

(c) Transition region

Figure 3.6: HE staining of a representative tumor

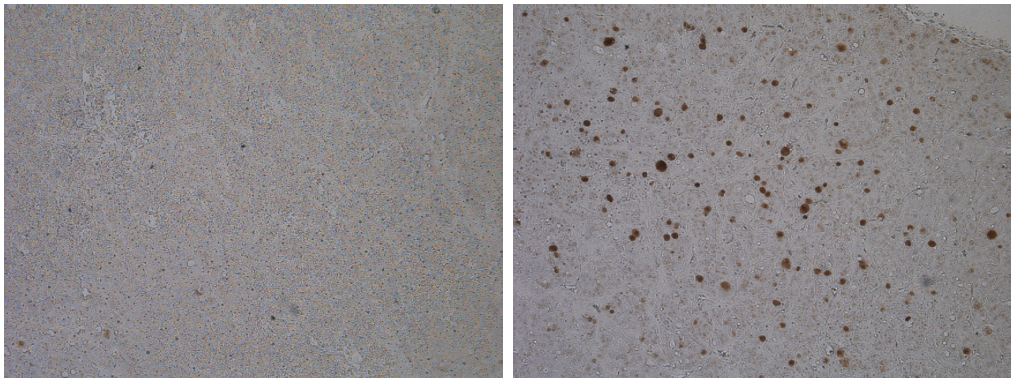

(a) UT

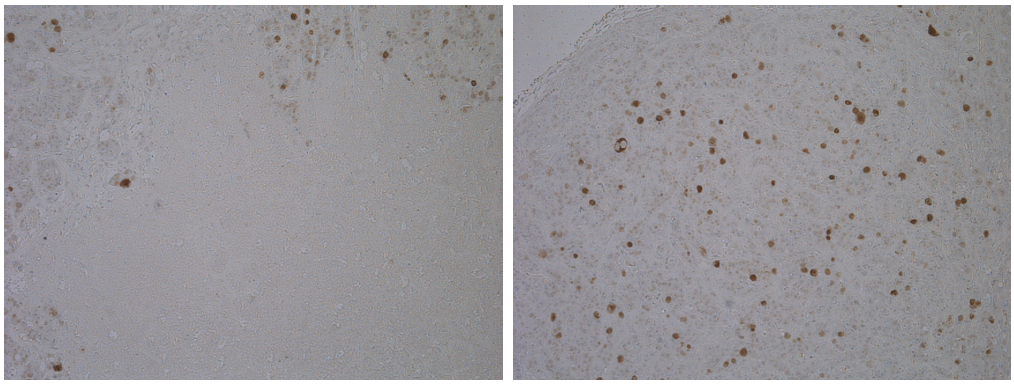

(b) TT

Figure 3.7: Ki67 staining of a representative UT and TT. Unproliferative (left) and proliferative (right) regions.

3.2.4 CD-68 (inflammation) and CD-34 (vasculature)

Unfortunately, neither CD-68 nor CD-34 staining yielded useful results. We observed unspecific staining in the negative control (no primary antibody) which correlated with the specifically stained regions observed. The staining was located mostly in the necrotic areas of the tumors. This unspecific staining was thought to be due to the secondary antibody that may have recognized regions of binding within the tissue. A different secondary antibody was also assessed and showed no unspecific staining, but no specific staining as well. The IHC experiments were repeated several times, but due to time constraints they could not be further assessed. The antibodies and protocols for these IHCs thus require further improvements to enable this type of staining.

3.3 Bioluminescence Imaging

We observed a steady growth of tumors from day 2 on that was similar for both left and right tumors (Figure 3.8(a), (b), and (c)). Immediately after RT, no clear difference was observed between TTs and UTs (Figure 3.8(d) and (e)). The effects of RT began to be visible on day 23 (9 days after RT) where there was a decrease in BLI signal in TTs (Figure 3.8(f) and (g) left) compared to UTs that continued their growth (Figure 3.8(f) and (g) right).

Interestingly, UTs on treated mice were smaller and gave a lower BLI signal than the completely unirradiated control tumors (Figure 3.9). This was explained by the fact that the lead shield used to protect the rest of the mouse body during tumor irradiation was not thick enough to block all the radiation. The thickness of the lead shield was $1/8\,inch$ ($3.175\,mm$), and about 10% of the dose went through the lead, therefore UTs received about $1\,Gy$ or $2\,Gy$ for the $10\,Gy$ or $20\,Gy$ group, respectively. In order to block 99% of radiation, this thickness should be doubled to $1/4\,inch$.

Figure 3.10 shows tumor growth and RT response for the different groups graphically. We observed a stable increase in BLI signal during the first 2 weeks after inoculation. The BLI signal difference between TTs, UTs, and controls appeared on day 23 (9 days after treatment) and was further enhanced on day 30

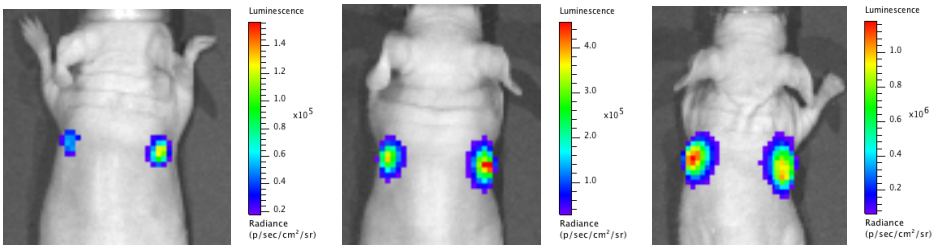

(a) Day 2 (b) Day 8 (c) Day 13

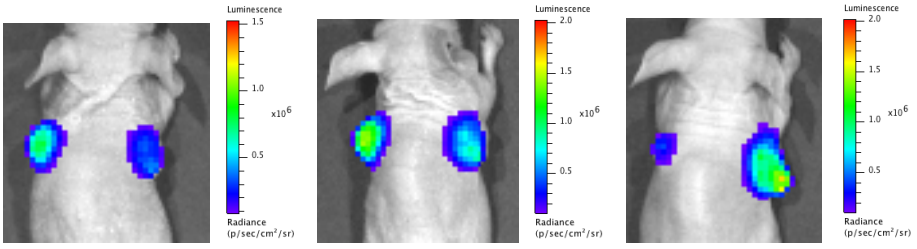

(d) Day 15 (e) Day 17 (f) Day 23

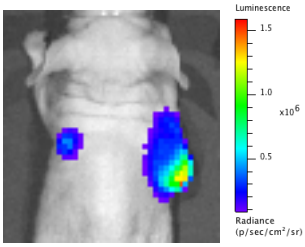

(g) Day 30

Figure 3.8: BLI of a representative mouse that received a dose of 10 Gy to the left tumor on day 14.

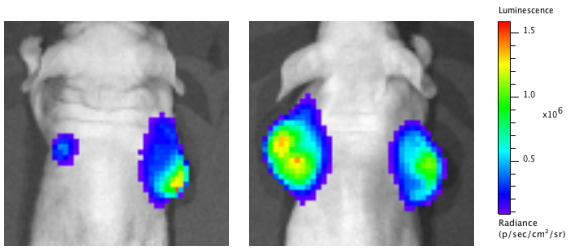

(a) TT and UT (b) Control

Figure 3.9: Comparison between TT, UT and unirradiated control tumors.

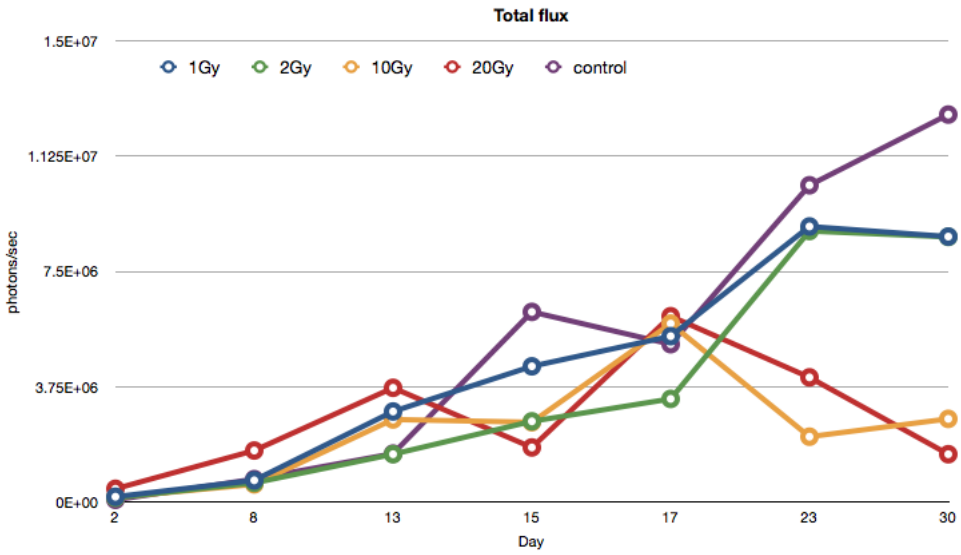

Figure 3.10: Monitoring of tumor growth and response to RT (delivered on day 14) for different doses.

(16 days post RT). The completely unirradiated control tumors showed a steady increase in BLI signal with the highest signal intensity observed on day 23 and 30 (Figure 3.10, purple line). The UTs that still received $1\,Gy$ or $2\,Gy$ showed a higher signal than the TTs but lower than the controls (Figure 3.10, blue and green lines). The TTs demonstrated a clear decrease in signal after RT, but no observable difference was noticed between $10\,Gy$ and $20\,Gy$, except that the TTs with $10\,Gy$ went up again whereas the $20\,Gy$ continued their decrease on day 30 (Figure 3.10, red and yellow lines).

Chapter 4

Discussion

In this study, we imaged a colorectal carcinoma xenograft mouse model before and after 10 and 20 Gy of RT with FDG-PET-CT and BLI. We showed an increased FDG uptake with PET 9 days after treatment, which was probably due to inflammation. We also demonstrated a stabilization (with 10 Gy) or decrease (with 20 Gy) in tumor size with CT, as well as a clear decrease in BLI signal in treated tumors which was also apparent 9 days after RT.

4.1 TTs volume stabilized or decreased whereas UTs continued their growth

When tumors were treated with RT, there was a clear difference in tumor size compared to UT as shown by both CT and BLI. There was a decrease in TT volume, which was visible on CT images, only in tumors treated with 20 Gy, whereas we only reached a state of tumor control (i.e. volume remained static) when treated with 10 Gy. Those results were detected earlier during the follow up period (day 9) for the smaller tumors compared with the bigger tumors (day 14). The tumor size was also assessed with histology. It was shown for the big tumors that TTs treated with a dose of 20 Gy were smaller than those treated with 10 Gy. In addition, a clear decrease in TTs BLI signal was visible starting 9 days after treatment and remained 16 days after RT. No difference in BLI signal was observed when comparing tumors treated with 10 or 20 Gy.

Interestingly, due to a too thin lead shield used during RT, UTs also received a dose of 1 or 2 Gy and showed therefore a smaller size compared to completely untreated controls. This was visible with BLI, where those tumors showed more signal than the TTs that got 10 or 20 Gy, but a lower signal than the unirradiated controls. These results were not observed with CT imaging, and showed how BLI is far more sensitive than anatomical CT imaging in this case for treatment assessment monitoring.

4.2 Increased FDG uptake after RT

The studied xenograft model showed a very low tumor FDG uptake on the baseline PET scans before treatment, regardless of tumor size. Surprisingly, an increase in FDG uptake in TTs was observed on day 9 after RT for all TTs, followed by decrease for some tumors or stabilization for others on day 14. Despite the tumor volumes remaining unchanged in TTs, PET images showed a strong increase in signal in response to RT.

Different hypotheses to explain this increase were assessed with histology. The most likely hypothesis was inflammation following RT, but accelerated repopulation and angiogenesis were also considered possible hypotheses. Proliferation was assessed with Ki67 staining, which highlighted tumor heterogeneities with an unproliferative center surrounded by a rim of proliferation. These findings were reflecting the hematoxylin and eosin staining that showed a necrotic center with viable tumor cells on the edge. However, this was common to both treated and untreated tumors. We could therefore conclude that the increased FDG uptake was not due to accelerated repopulation following RT. Unfortunately, the immunohistochemistry for inflammation and angiogenesis (CD-68 and CD-34 staining, respectively) did not provide meaningful results. Different antibodies could be further assessed and the protocol remains to be improved in order to enable staining for these proteins.

Nevertheless, inflammation seems to be the most likely reason for this increase in FDG uptake, as described in the literature. Indeed, higher FDG uptake was observed early on in response to RT [25, 26, 7]. It is known that macrophages and other activated immune cells within the tumor take up FDG more than normal

tissue [27]. After RT, immune cells can be recruited to infiltrate the tumor, therefore increasing the FDG uptake. This phenomenon is well known and has been exploited to image different inflammatory processes such as atherosclerotic plaques [28, 29] and infection [30]. FLT, a PET tracer that assesses proliferation, has been proposed as an alternative to FDG to differentiate tumor cells from inflammation [31]. Another option is dual time point imaging with FDG, with early and delayed scans where benign inflammatory processes should give varying and transient signal compared to more stable signal for malignant lesions [32].

FDG is an unspecific tracer, and hence changes in its uptake level and distribution have to be assessed with caution. Imaging with FDG-PET early on after RT, or even during treatment if RT is fractionated, can show changes in signal that do not always correspond to the outcome of the response. Indeed, in a tumor that is taking up FDG on the baseline scan, any increase in PET signal above the baseline signal early after RT can be misinterpreted as a radioresistant or unresponsive tumor. The results of follow up scans therefore have to be interpreted with the possibility of false negatives from inflammation in mind. Several studies have reported decreased FDG uptake after treatment both pre-clinically [8] and clinically [5, 33], this making FDG-PET a good method for assessing response. In some cases however, FDG-PET may not be the optimal imaging modality to assess early changes in tumor response to RT.

Chapter 5

Conclusion

5.1 Research perspectives

This study provided interesting views on the time scale, dose and tumor size influence of events occurring after RT with respect to imaging. The study had some limitations, for example the limited number of mice studied in different groups that made the statistical significance of the results hard to reach.

The cell line used here did not strongly take up FDG, so a similar study with different cell lines that exhibit a stronger FDG-PET signal would facilitate the study of early response effects. Also, a subcutaneous tumor model was used, which is known to be different to tumors growing in their native environment [34]. It would be interesting to repeat a similar study with orthotopic or spontaneously occurring tumors.

Furthermore, we tested RT delivered as a single fraction, which differs significantly from the fractionated regimens that are used clinically, and this could have led to some differences in molecular response. A fractionated study with the delivery of multiple low doses of RT would give a better understanding of the influence of fractionation in imaging tumor response. Another question raised by those results is the fact that RT was delivered with a single field irradiator with a lead shield to protect the mouse body from radiation which was not thick enough to block all the dose. It would be worth repeating the experiments with a thicker shield to make sure that the untreated tumor does not receive any significant dose.

In addition, the use of a conformal microCT (able to deliver radiation from multiple angles), would be interesting in that we would get a result closer to the clinical situation [35]. Thus far, the dose rate achieved with this system is lower than the single field irradiator which would not only mean that big studies involving many mice would be very time consuming, but also that the radiobiology of molecular effects would be different.

Finally, investigating tumor response to RT with other imaging modalities would bring supplementary important molecular aspects in the picture. An example would be the use of a fluorescent peptide that binds to integrins [36] to study the effects of RT on tumor vasculature and angiogenesis. We could also consider imaging with different PET tracers that would allow the understanding mechanisms such as proliferation with FLT, or hypoxia with EF5.

5.2 Conclusion

Imaging and radiation oncology are closely interconnected, especially at the treatment planning level. Assessment of tumor response to RT is a growing and active field of research, which aims at a better and more patient specific treatment of cancer. Identifying and understanding the early molecular events occurring after RT would allow improved interpretation of images. Indeed, being able to detect false negatives (i.e. differentiate between events such as inflammation and radioresistance) early on with non-invasive imaging would allow for an adaptation of the treatment protocol, which could directly benefit the patients.

This study provided an insight of the complexity of imaging tumor response to radiotherapy and highlighted the research efforts that still remain to be performed in this field.

Appendix A

Cell culture

A.1 Cell medium change & Splitting

The growth medium for the cells was Mc Coy's Medium with 10% fetal bovine serum (FBS) in 5% CO_2 at 37°C in a humidified incubator. Cell culture manipulations were performed under a fume hood.

Cells were thawed and seeded on a 10cm cell culture dish with 20ml of growth media and kept in an incubator.

Growth media was changed three times a week by removing the media and adding 20ml of fresh media in the cell culture dish .

When the dish was confluent, about once a week, cells were split in two dishes. The culture media was removed and cells were rinsed with 5ml of PBS. Then 5ml trypsin was added, and left for a few minutes in the incubator until cells were well detached. Cells were mixed by pipetting up and down, and the desired quantity was then seeded on a new dish, with fresh growth media, and kept in the incubator.

A.2 Cell counting

Cell counting was performed every time the amount of cells needed to be assessed for further experiments. Growth media was removed and cells were rinsed with 5ml PBS. 5ml of trypsin was added and cells were left in incubator for 5 minutes until cells were detached. Detached cells together with trypsin were mixed by pipetting up and down and added to 25ml of growth media in a tube so the total volume was 30ml. In a small well, 40 μl of trypan blue (stain used for the visualization of alive cells) and 10μl of cells from tube were added and mixed. 10μl of which were introduced in a Neubauer chamber. Under the microscope, cells present in squares of the Neubauer chamber were counted. The number of cells per ml can then be deduced by using the following formula:

$$\frac{c \cdot v \cdot d \cdot 1000}{s}$$

where c is the number of counted cells, v is the volume in the chamber (here $10\mu l$), d is the dilution (here 5), 1000 is to convert to ml, and s is the number of squares (here 9).

Knowing the concentration of cells, it was then possible to centrifuge and resuspend the cells in an appropriate volume of culture media for further use.

A.3 Cell freezing

In order to keep cells for further purposes, some cells were frozen. Cells were counted, centrifuged at 1300 rpm at room temperature for 5 minutes, and re-suspended in an appropriate volume of Fetal Bovine serum (FBS) with 10% of DMSO (cryo protective agent). Cells were subsequently stored in a cryo freezing container at -80°C.

Appendix B

Immunohistochemistry

B.1 Ki67 staining Procedure Avidin Biotin (Peroxidase method)

Everything at Room Temp unless otherwise specified

1. Dewax with xylene about 10-15 minutes.
2. Rehydrated

   Absolut EtOH 5 min

   95°C EtOh 5 min

   85°C EtOH 5min

   70°C EtOH 5min

   H2Od 5 min
3. Antigen retrieval with 10mM Citric Acid pH=6. 2-3 minutes in a microwave (repeat 3 or 4 times). Cool till RT (around 20 minutes)
4. Rinse in 1x PBS 3 x 5min.

5. Peroxidase quenching with 3% H2O2 (4.3ml of 35% H2O2 in 50 ml of PBS 1X) for 10 minutes
6. Rinse in tap water
7. Humid Chamber (Tip box)
8. Wash 3 times with PBS 1X
9. Avidin Biotin quenching using Avidin D Biotin (solution) for 5 minutes.
10. Rinse in PBS
11. Block with Biotin blocking reagent at RT
12. Rinse in PBS
13. Apply 10% blocking serum (goat) 0.1% Tween/ PBS mixture for 1h. PBS-Tween 0.1%-Serum10%
14. Apply Primary Antibody/ Blocking Serum (same as above) mixture (1:250) in Cold Room (4°C). Leave Overnight; PBS-Tween 0.1%-%-Ab
15. Rinse in 1x PBS 3 x 5min (or PBS-Tween 0.1% and last with PBS). For the last PBS I preferable to wash out the soap
16. Apply Secondary biotinylated Antibody / Blocking Serum (same as above) mixture (1:200) for 1 hr. PBS-Tween 0.1%-Serum1%-Ab 2nd. Biotin-Avidin/Streptavidin system amplifies the signal as each Biotin molecule binds 6 Avidin/Streptavidin molecules.
17. Rinse in 1x PBS 3 x 5min in cup (or PBS-Tween 0.1% and last with PBS)
18. Dilute the third Avidin/Stretavidin antibody conjugated to HRP or fluorochrome in blocking solution (1:200) and incubate at room temperature for 30-45 minutes
19. Wash 3 times for 5 minutes with PBS 1X

20. Develop signal (Vector Laboratories DAB substrate Kit for Peroxidase). Bring the solution to RT and add one drop of DAB to 1 ml of substrate. Mix well. Apply this solution at RT and monitor signal development as soon as some signal is seen
21. Wash sections for 5 minutes in distilled water.
22. Immerse very quickly in Haematoxylin
23. Rinse in water
24. Mount with Fluoromount-G with anti-fading agents

References

[1] A.A. Neves and K.M. Brindle. Assessing responses to cancer therapy using molecular imaging. *BBA-Reviews on Cancer*, 1766(2):242–261, 2006. 2

[2] K. Brindle. New approaches for imaging tumour responses to treatment. *Nature Reviews Cancer*, 8(2):94–107, 2008. 2

[3] R.J. Hicks. Role of 18F-FDG PET in assessment of response in non-small cell lung cancer. *Journal of Nuclear Medicine*, 50(Suppl_1):31S, 2009. 2

[4] J.K. Schwarz, P.W. Grigsby, F. Dehdashti, and D. Delbeke. The role of 18F-FDG PET in assessing therapy response in cancer of the cervix and ovaries. *Journal of Nuclear Medicine*, 50(Suppl_1):64S, 2009. 2

[5] L.F. de Geus-Oei, D. Vriens, H.W.M. van Laarhoven, W.T.A. van der Graaf, and W.J.G. Oyen. Monitoring and predicting response to therapy with 18F-FDG PET in colorectal cancer: a systematic review. *Journal of Nuclear Medicine*, 50(Suppl_1):43S, 2009. 2, 29

[6] M.H. Pan, S.C. Huang, Y.P. Liao, D. Schaue, C.C. Wang, D.B. Stout, J.R. Barrio, and W.H. McBride. FLT-PET imaging of radiation responses in murine tumors. *Molecular Imaging and Biology*, 10(6):325–334, 2008. 2

[7] C. Murayama, N. Harada, T. Kakiuchi, D. Fukumoto, A. Kamijo, A.T. Kawaguchi, and H. Tsukada. Evaluation of D-18F-FMT, 18F-FDG, L-11C-MET, and 18F-FLT for Monitoring the Response of Tumors to Radiotherapy in Mice. *Journal of Nuclear Medicine*, 50(2):290, 2009. 2, 7, 28

[8] C.F.M. Molthoff, B.M. Klabbers, J. Berkhof, J.T. Felten, M. Van Gelder, A.D. Windhorst, B.J. Slotman, and A.A. Lammertsma. Monitoring Response to Radiotherapy in Human Squamous Cell Cancer Bearing Nude Mice: Comparison of 2′deoxy-2′[18 F] fluoro-d-glucose (FDG) and 3′[18 F] fluoro-3′deoxythymidine (FLT). *Molecular Imaging and Biology*, 9(6):340–347, 2007. 2, 29

[9] P. Vaupel. Tumor microenvironmental physiology and its implications for radiation oncology. In *Seminars in radiation oncology*, volume 14, pages 198–206. Elsevier, 2004. 2

[10] EE Graves and AJ Giaccia. Imaging tumoral hypoxia: oxygen concentrations and beyond. *Oncology (Williston Park, NY)*, 21(3):368, 2007. 3

[11] T. Seierstad, K. Rře, and D.R. Olsen. Noninvasive monitoring of radiation-induced treatment response using proton magnetic resonance spectroscopy and diffusion-weighted magnetic resonance imaging in a colorectal tumor model. *Radiotherapy and Oncology*, 85(2):187–194, 2007. 3

[12] R.M. Vlad, S. Brand, A. Giles, M.C. Kolios, and G.J. Czarnota. Quantitative ultrasound characterization of responses to radiotherapy in cancer mouse models. *Clinical Cancer Research*, 15(6):2067, 2009. 3

[13] C.H. Contag, D. Jenkins, P.R. Contag, and R.S. Negrin. Use of reporter genes for optical measurements of neoplastic disease in vivo. *Neoplasia (New York, NY)*, 2(1–2):41, 2002. 3, 5

[14] M. Edinger, T.J. Sweeney, A.A. Tucker, A.B. Olomu, R.S. Negrin, and C.H. Contag. Noninvasive assessment of tumor cell proliferation in animal models. *Neoplasia (New York, NY)*, 1(4):303, 1999. 3

[15] D.A. Mankoff. A definition of molecular imaging. *Journal of Nuclear Medicine*, 48(6):18N, 2007. 3

[16] J.M. Ollinger and J.A. Fessler. Positron-emission tomography. *IEEE Signal Processing Magazine*, 14(1):43–55, 1997. 4

[17] S. Vallabhajosula. 18F-labeled positron emission tomographic radiopharmaceuticals in oncology: an overview of radiochemistry and mechanisms of tumor localization. In *Seminars in Nuclear Medicine*, volume 37, pages 400–419. Elsevier, 2007. 4

[18] G. Delaney, S. Jacob, C. Featherstone, and M. Barton. The role of radiotherapy in cancer treatment. *Cancer*, 104(6):1129–1137, 2005. 5

[19] E.J. Hall and A.J. Giaccia. *Radiobiology for the Radiologist*. Lippincott Williams & Wilkins, 2006. 6

[20] M.C. Joiner and AJ Van der Kogel. Basic clinical radiobiology. *Particle Beams in Radiotherapy*, pages 173–183, 1997. 6

[21] Q. Cao, W. Cai, G. Niu, L. He, and X. Chen. Multimodality imaging of IL-18–binding protein-Fc therapy of experimental lung metastasis. *Clinical Cancer Research*, 14(19):6137, 2008. 7

[22] C. Schutze, R. Bergmann, A. Yaromina, F. Hessel, J. Kotzerke, J. Steinbach, M. Baumann, and B. Beuthien-Baumann. Effect of increase of radiation dose on local control relates to pre-treatment FDG uptake in FaDu tumours in nude mice. *Radiotherapy and Oncology*, 83(3):311–315, 2007. 7

[23] E.E. GRAVES, A. QUON, and B.W. LOO. RT_Image: an open-source tool for investigating PET in radiation oncology. *Technology in cancer research & treatment*, 6(2):111–121, 2007. 11

[24] S. Vallabhajosula. *Molecular Imaging: Radiopharmaceuticals for PET and SPECT*. Springer Verlag, 2009. 11

[25] H. Hautzel and H.W. Muller-Gartner. Early changes in fluorine-18-FDG uptake during radiotherapy. *Journal of Nuclear Medicine*, 38(9):1384, 1997. 28

[26] M. Furuta, M. Hasegawa, K. Hayakawa, M. Yamakawa, H. Ishikawa, T. Nonaka, N. Mitsuhashi, and H. Niibe. Rapid rise in FDG uptake in an irradiated human tumour xenograft. *European Journal of Nuclear Medicine and Molecular Imaging*, 24(4):435–438, 1997. 28

[27] R. Kubota, S. Yamada, K. Kubota, K. Ishiwata, N. Tamahashi, and T. Ido. Intratumoral distribution of fluorine-18-fluorodeoxyglucose in vivo: high accumulation in macrophages and granulation tissues studied by microautoradiography. *Journal of Nuclear Medicine*, 33(11):1972, 1992. 29

[28] JHF Rudd, EA Warburton, TD Fryer, HA Jones, JC Clark, N. Antoun, P. Johnstrom, AP Davenport, PJ Kirkpatrick, B.N. Arch, et al. Imaging atherosclerotic plaque inflammation with [18F]-fluorodeoxyglucose positron emission tomography. *Circulation*, 105(23):2708, 2002. 29

[29] A. Tawakol, R.Q. Migrino, G.G. Bashian, S. Bedri, D. Vermylen, R.C. Cury, D. Yates, G.M. LaMuraglia, K. Furie, S. Houser, et al. In vivo 18F-fluorodeoxyglucose positron emission tomography imaging provides a noninvasive measure of carotid plaque inflammation in patients. *Journal of the American College of Cardiology*, 48(9):1818–1824, 2006. 29

[30] H. Zhuang and A. Alavi. 18-Fluorodeoxyglucose positron emission tomographic imaging in the detection and monitoring of infection and inflammation. In *Seminars in nuclear medicine*, volume 32, pages 47–59. Elsevier, 2002. 29

[31] A. van Waarde, D.C.P. Cobben, A.J.H. Suurmeijer, B. Maas, W. Vaalburg, E.F.J. de Vries, P.L. Jager, H.J. Hoekstra, and P.H. Elsinga. Selectivity of 18F-FLT and 18F-FDG for differentiating tumor from inflammation in a rodent model. *Journal of Nuclear Medicine*, 45(4):695, 2004. 29

[32] H. Zhuang, M. Pourdehnad, E.S. Lambright, A.J. Yamamoto, M. Lanuti, P. Li, P.D. Mozley, M.D. Rossman, S.M. Albelda, and A. Alavi. Dual time point 18F-FDG PET imaging for differentiating malignant from inflammatory processes. *Journal of Nuclear Medicine*, 42(9):1412, 2001. 29

[33] S.D. Rege, L. Chaiken, C.K. Hoh, Y. Choi, R. Lufkin, Y. Anzai, G. Juillard, J. Maddahi, ME Phelps, and RA Hawkins. Change induced by radiation therapy in FDG uptake in normal and malignant structures of the head and neck: quantitation with PET. *Radiology*, 189(3):807, 1993. 29

[34] E.E. Graves, M. Vilalta, I. Cecic, J.T. Erler, P.T. Tran, D. Felsher, L. Sayles, A. Sweet-Cordero, Q.T. Le, and A.J. Giaccia. Hypoxia in Models of Lung Cancer: Implications for Targeted Therapeutics. *Clinical Cancer Research*, In press. 30

[35] M. Rodriguez, H. Zhou, P. Keall, and E. Graves. Commissioning of a novel microCT/RT system for small animal conformal radiotherapy. *Physics in Medicine and Biology*, 54:3727–3740, 2009. 31

[36] R.H. Kimura, Z. Cheng, S.S. Gambhir, and J.R. Cochran. Engineered knottin peptides: a new class of agents for imaging integrin expression in living subjects. *Cancer research*, 69(6):2435, 2009. 31